Optical squeezing mediated by levitated oscillators at their quantum ground state

A. Pontin [1,*] Q. Deplano [2,3] F. Marino [1,3] and F. Marin [1,2,3,4,†]
[1] *CNR-INO, Largo Enrico Fermi 6, I-50125 Firenze, Italy*
[2] *Dipartimento di Fisica e Astronomia, Università di Firenze, via Sansone 1, I-50019 Sesto Fiorentino, Italy*
[3] *INFN, Sezione di Firenze, via Sansone 1, I-50019 Sesto Fiorentino, Italy*
[4] *European Laboratory for Non-Linear Spectroscopy (LENS), Via Carrara 1, I-50019 Sesto Fiorentino, Italy*

(Received 29 April 2026; accepted 13 October 2026; published 4 November 2026)

We demonstrate optical squeezing below the shot-noise level generated through the interaction of an optical cavity field with two center-of-mass modes of a levitated nanoparticle, simultaneously cooled to occupation numbers well below unity. By analyzing the quadrature fluctuations of the cavity output through heterodyne detection, we resolve the full spectral covariance matrix of the optical field and map regions of sub-shot-noise squeezing as a function of detection phase and frequency. Operating in the resolved sideband and strong-coupling regime where mechanical modes hybridize with the optical mode, we observe consistent squeezing in the band 70–95 kHz with a lowest variance of 0.98 (2% below vacuum fluctuations). We thus demonstrate optical squeezing mediated by multiple mechanical oscillators in their quantum ground state, bridging mechanical quantum control with nonclassical light and establishing levitated optomechanics as a platform for multimode quantum interactions.

DOI: 10.1103/hms3-yb2h

I. INTRODUCTION

At the dawn of cavity optomechanics the two major experimental milestones, which remained elusive for a long time, were the ground-state cooling of a macroscopic mechanical oscillator and the generation of so-called ponderomotive squeezing. The latter arises when quantum correlations in the quadratures of an optical field, induced by an optomechanical interaction, allow the achievement of sub-shot-noise fluctuations [1,2]. These two objectives have since been accomplished [3,4], but the fact remains that they have mutually exclusive favorable regimes: Motional cooling is enhanced in the resolved sideband regime [5], while ponderomotive squeezing is better observed in the bad-cavity regime [1]. The field has since significantly progressed, with the observation of a range of quantum phenomena, from the measurement of an oscillator motion near the Heisenberg limit [6], to multimode [7] and room-temperature [8] squeezing, and even more deeply nonclassical phenomena [9,10].

Despite these advances, a key challenge remains largely unaddressed: the simultaneous observation of quantum behavior in both the mechanical and optical subsystems. This is particularly demanding because, as discussed above, the regimes favoring motional ground-state cooling and ponderomotive squeezing are generally different. Most demonstrations of ponderomotive squeezing have not prepared a quantum mechanical oscillator, as indeed a classical oscillator suffices. Combining optical squeezing with a mechanical mode cooled below unit occupation brings the system into a regime where both subsystems simultaneously display quantum behavior, providing the conditions required for the generation of genuinely joint mechanical-optical nonclassical states [11–13].

Here, we demonstrate optical squeezing below shot noise, mediated by the interaction between an optical cavity field and two center-of-mass modes of a levitated nanoparticle, each cooled to occupation numbers substantially below unity. Levitated optomechanics has recently emerged as a versatile platform and a promising avenue for sensing, both for fundamental science [14–16] and technological applications [17]. In the context of the two optomechanical milestones discussed above, ground-state cooling has been achieved for a single [18–23] and two oscillating modes [24,25] and squeezed light has been observed [26,27], notably, without using an optical cavity. The simultaneous quantum behavior of the mechanical and optical subsystems demonstrated here shows that levitated optomechanics can access this challenging regime. Its relevance for quantum-state engineering has recently been demonstrated in a similar system, where the introduction of an additional two-mode-squeezing interaction enabled mechanical-optical entanglement [28], opening the way to applications such as mechanical oscillators acting as local quantum memories [29,30].

The experimental system on which this work is based is presented in Ref. [25], where the focus is on the properties of the mechanical subsystem. Here, we analyze the same experimental data to derive the quantum properties of the optical field at the output of the cavity. Crucially, the

*Contact author: antonio.pontin@cnr.it
†Contact author: francesco.marin@unifi.it

Published by the American Physical Society under the terms of the Creative Commons Attribution 4.0 International license. Further distribution of this work must maintain attribution to the author(s) and the published article's title, journal citation, and DOI.

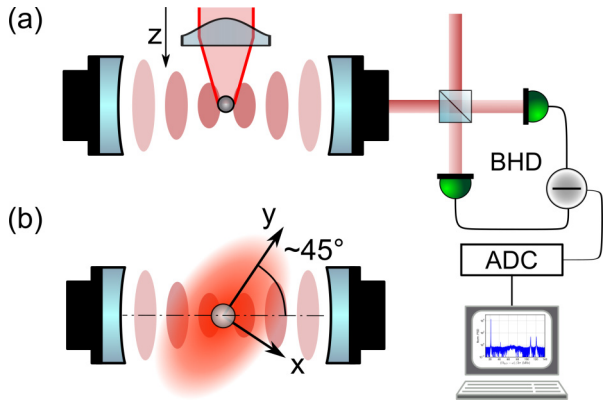


FIG. 1. Pictorial view of the experiment. (a) An optical tweezer confines a silica nanosphere. The particle is positioned at the center of an optical cavity, near a node of the intracavity standing wave. The cavity output field is analyzed by a balanced heterodyne detection (BHD) whose output is acquired through an analog-to-digital converter (ADC). (b) The tweezer focus is slightly elliptical in the transverse plane with major (y) and minor (x) axes rotated by $\sim 45^\circ$ from the cavity axis.

system operates in the resolved sideband regime, which is far less favorable for the observation of squeezing, and in the strong-coupling regime where optical and mechanical modes hybridize. Nonetheless, the underlying mechanism responsible for the generation of squeezed light is the conventional one [1,2]: Quantum fluctuations of the optical field drive the mechanical motion, which is then imprinted back onto the optical field. By analyzing the quadrature fluctuations of the cavity output field through heterodyne detection, we resolve the full spectral covariance matrix of the optical field and map regions of sub-shot-noise squeezing as a function of detection phase and frequency. While squeezing can be generated using a single mechanical mode, reaching the motional ground state requires addressing the intrinsically two-dimensional (2D) nature of the motion. [25,31]. These results demonstrate a regime in which nonclassical optical fluctuations emerge from the collective dynamics of two not-independent mechanical modes in the quantum regime. Furthermore, optomechanical hybridization goes beyond a description in terms of independent oscillators, and highlights the role of multimode quantum dynamics in shaping the optical field.

II. EXPERIMENTAL SETUP

A schematic view of the setup is shown in Fig. 1. It is based on a coherent scattering approach [18,32] where a silica nanoparticle, confined in an optical tweezer, is placed at the center of an empty high-finesse cavity. Light scattered by the particle populates the cavity mode when the tweezer field is resonant with the cavity. The resulting interference creates a much larger coupling between the particle motion and the cavity field when compared to dispersive coupling [31,33]. A detailed description of the experimental setup can be found in Refs. [25,34], while here we summarize only its main aspects.

The optical tweezer provides a 3D trapping potential with frequencies $(\Omega_x, \Omega_y, \Omega_z)/2\pi \simeq (121, 109, 21)$ kHz. The motion in the transverse plane of the tweezer, x-y, is coupled to the cavity field with rates g_x and g_y, respectively, and is heated mainly by residual gas collisions and photon recoil. Their total effect is captured by the heating rates Γ_x and Γ_y. The motion along the tweezer propagation axis, z, can be safely neglected, since it is very weakly coupled to the cavity mode and there is a sufficiently large separation between mechanical resonances. The optical cavity has a full linewidth $\kappa/2\pi = 57$ kHz, and as such the transverse dynamics is well within the resolved sideband regime ($\Omega_i > \kappa/4$) [5]. Thus, setting an optimal detuning $-\Delta \simeq \Omega_i$ the cavity provides efficient motional cooling [35]. The cavity output field is analyzed through a balance heterodyne detection (BHD). The parameters that are experimentally determined, as reported in Ref. [25], are summarized in Table I. These allowed to estimate mean occupation numbers of $n_x = 0.55 \pm 0.03$ and $n_y = 0.74 \pm 0.04$, both well below the unity threshold [i.e., by 15 and 6.5 standard errors (σ), respectively].

TABLE I. System parameters determined in Ref. [25]: Coupling rates g_i between the cavity mode and particle motion in the tweezer transverse plane x-y, and the associated heating rates Γ_i. Measurements were performed at a pressure of $\sim 3 \times 10^{-8}$ mbar.

$g_x/2\pi$ (kHz)	$g_y/2\pi$ (kHz)	$\Gamma_x/2\pi$ (kHz)	$\Gamma_y/2\pi$ (kHz)
14.13 ± 0.22	10.37 ± 0.16	4.03 ± 0.32	3.05 ± 0.26

III. ANALYSIS

Having established the system parameters we now focus on the characteristics of the quadratures of the optical field measured at the output of the cavity. We are interested in observing squeezed light generated by the interaction with the levitated nanoparticle, that is, field fluctuations below the shot-noise level. Typically, this is verified by experimentally implementing a homodyne detection, which allows to analyze the fluctuations of a chosen field quadrature. In our case, however, the necessary phase-sensitive detection is reconstructed in postprocessing starting from time traces of the BHD. We implement a numerical lock-in amplifier that allows us to measure and stabilize the phase of the beat note in the heterodyne signal [28]. This approach allows us to reconstruct the complete spectral covariance matrix $\mathbf{V}_{QP}$ with elements $\mathrm{V}_{ij} = 0.5\langle\{\mathrm{u}_i, \mathrm{u}_j\}\rangle$ where $\mathbf{u} = (Q_m(\omega), P_m(\omega))$. Here, Q_m and P_m are the measured field quadratures in the frequency domain, normalized to the vacuum level, and $\{\cdot, \cdot\}$ indicates the anticommutator. A few considerations are in order: (i) The determination of $\mathbf{V}_{QP}$ is completely model independent; (ii) the phase references which determine the quadratures, both in the model and in $\mathbf{V}_{QP}$, are arbitrary and are chosen to match; (iii) the simultaneous measurement of the conjugate variables (Q_m, P_m) entails a noise penalty which in this context can be interpreted as an additional factor of 1/2 in the total detection efficiency η [36].

IV. RESULTS

We show in Fig. 2 the measured power spectral densities (PSDs) composing the elements of the matrix $\mathbf{V}_{QP}$. The total measurement time was 250 s, with a detection efficiency of

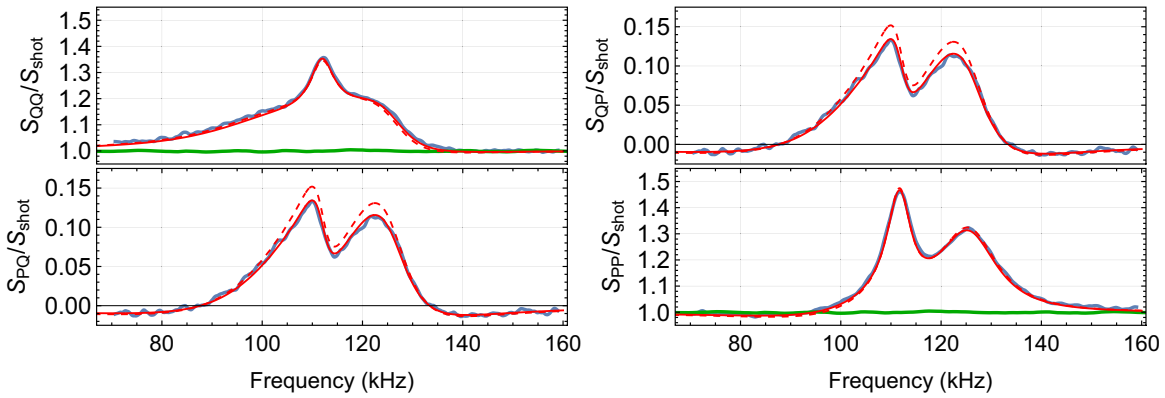


FIG. 2. Spectral covariance matrix. Fluctuations of the cavity output field quadratures are reconstructed from a balanced heterodyne measurement through a phase-sensitive analysis. The panels show all spectral elements of the measured covariance matrix $\mathbf{V}_{QP}$ (blue). The spectra are compared with model predictions assuming parameters from Table I, with (solid red) and without (dashed red) contribution from phase noise. The variance σ_θ^2 is obtained by fitting simultaneously the four spectra using Eq. (1) with σ_θ^2 as the only free parameter. The green line in the diagonal elements indicates the independently measured vacuum fluctuations used for calibration.

$\eta = 0.32$ (without the additional factor $1/2$ mentioned above). Interestingly, the shape of the diagonal elements, i.e., the PSD of the quadratures $S_{Q_mQ_m}$ and $S_{P_mP_m}$, differ significantly from a pair of Lorentzian peaks. This is a direct consequence of the strong-coupling regime, where the mechanical modes are hybridized with the optical one. Indeed, it can be shown that, when the cavity detuning is scanned across the mechanical modes resonances, the parameters of Table I lead to a double avoided crossing [34,37], producing nontrivial spectral shapes that also exhibit quantum features [25,34,38].

A comparison between the experiment and the calculated PSDs (see Ref. [25] and Appendix A) using the parameters obtained in Ref. [25], however, shows small discrepancies. This is more evident for the off-diagonal PSDs, while good agreement remains along the diagonal. This behavior leads us to conjecture a residual phase noise affecting the determination of the optical quadratures. We model it by considering a fluctuating phase θ, Gaussian distributed with variance σ_θ^2, over which the analytical covariance matrix needs to be averaged. To this end, we consider a rotation of the covariance matrix as $\mathbf{V}_{QP}^{\theta}(\theta) = \mathbf{R}(\theta)\mathbf{V}_{QP}\mathbf{R}(\theta)^T$, where $\mathbf{R}$ is a rotation matrix, and average over realizations of θ according to

$$\tilde{\mathbf{V}}_{QP} = \frac{1}{\sqrt{2\pi}\sigma_\theta}\int_{-\infty}^{\infty}\mathbf{V}_{QP}^{\theta}(\theta)\exp\left(-\frac{\theta^2}{2\sigma_\theta^2}\right)\mathrm{d}\theta.$$

It can be explicitly written as

$$\tilde{\mathbf{V}}_{QP} = e^{-\sigma_\theta^2}\begin{pmatrix} S_{PP}\sinh\left(\sigma_\theta^2\right) + S_{QQ}\cosh\left(\sigma_\theta^2\right) & S_{QP}\cosh\left(\sigma_\theta^2\right) - S_{PQ}\sinh\left(\sigma_\theta^2\right) \\ S_{PQ}\cosh\left(\sigma_\theta^2\right) - S_{QP}\sinh\left(\sigma_\theta^2\right) & S_{QQ}\sinh\left(\sigma_\theta^2\right) + S_{PP}\cosh\left(\sigma_\theta^2\right)\end{pmatrix}. \tag{1}$$

We fit the experimental data with Eq. (1) to determine the unknown variance σ_θ^2, which is the only free parameter. All other parameters necessary for the evaluation of the model have been fixed to the nominal values in Table I. As shown in Fig. 2, the agreement drastically improves, supporting the phase noise assumption. The fit returns a variance value of $\sigma_\theta^2 = 0.062\ \mathrm{rad}^2$.

Having reconstructed the covariance matrix $\tilde{\mathbf{V}}_{QP}$ it is straightforward to obtain the quadrature spectrum $\tilde{S}_Q^{\phi}$ for an arbitrary detection phase ϕ, through the transformation $\tilde{\mathbf{V}}_{QP}(\phi) = \mathbf{R}(\phi)\tilde{\mathbf{V}}_{QP}\mathbf{R}(\phi)^T$. This can be written in simple form, even in the presence of phase noise, as

$$\tilde{S}_Q^{\phi} = \tilde{V}_{QP}(1,1) = \frac{S_{QQ}+S_{PP}}{2} + \frac{S_{QQ}-S_{PP}}{2}e^{-2\sigma_\theta^2}\cos(2\phi) + S_{QP}\,e^{-2\sigma_\theta^2}\sin(2\phi), \tag{2}$$

where $\tilde{V}_{QP}(1,1)$ denotes the (1,1) element of $\tilde{\mathbf{V}}_{QP}$. Using Eq. (2) we can construct a 2D map showing the quadrature spectrum in a frequency bandwidth accross the x and y mode resonances, as a function of the phase ϕ, akin to a tomographic homodyne measurement. The resulting experimental map is shown in Fig. 3(a) where it is also compared with the model prediction [Fig. 3(b)]. The color code in the maps is chosen to clearly separate regions with sub-shot-noise statistics (blue scale). Two such regions are evident, in agreement with the model predictions.

A more direct and quantitative way to condense the information displayed in Fig. 3 is to evaluate the optimal squeezing spectrum $\tilde{S}_Q^{\mathrm{opt}}$, where the detection phase ϕ is optimized at every frequency [39]. It can be written as

$$\tilde{S}_Q^{\mathrm{opt}}(\omega) = S_{QQ}(\omega) + S_{PP}(\omega) - e^{-2\sigma_\phi^2} \times \sqrt{[S_{QQ}(\omega) - S_{PP}(\omega)]^2 + 4[S_{QP}(\omega)]^2}. \tag{3}$$

The resulting optimal spectrum is shown in Fig. 4, where it is compared with model predictions. As for the quadratures, without considering the effect of phase noise (dashed line in Fig. 4) some discrepancies with the experimental spectrum

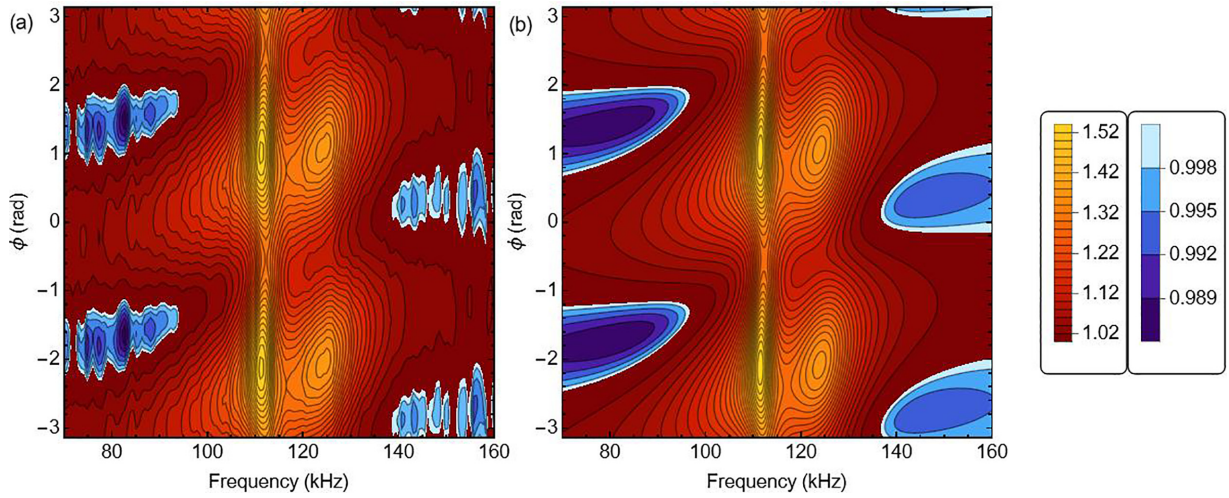


FIG. 3. 2D map of the optical quadrature spectrum as a function of the detection phase ϕ. (a) Experimental, model-independent map. (b) Model prediction of $\tilde{S}_Q^\phi$ including a phase noise contribution. In both maps, the color scale has been split into $\tilde{S}_Q^\phi > 1$ (red scale) and $\tilde{S}_Q^\phi < 1$ (blue scale) to highlight regions showing sub-shot-noise statistics. Two of such regions are evident, below the mechanical resonances (around 80 kHz) and above them (around 150 kHz). The corresponding detection phases are separated by $\simeq \pi/2$.

emerge. These are particularly evident around the peak at $\simeq$125 kHz. The agreement markedly improves when phase noise is included. However, in the regions where squeezing is observed, i.e., around 80 and 150 kHz, phase noise has a negligible effect. We point out that such remarkable agreement for the optimal spectrum implies that the agreement is quantitatively similar for any quadrature, at arbitrary detection phase ϕ.

V. DISCUSSION

The maximum observed squeezing is mild, but the spectrum is consistently below the shot noise between 70 and 95 kHz, with a lowest variance for a measured quadrature

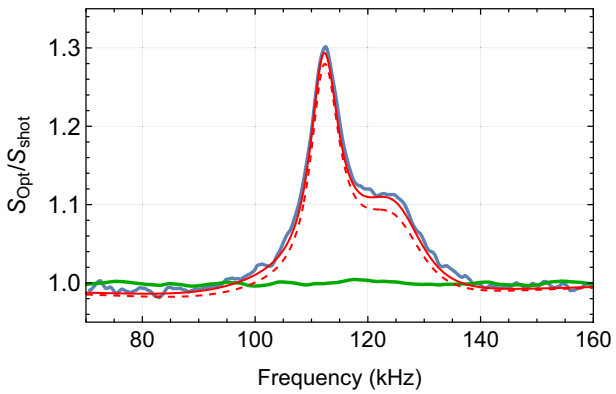


FIG. 4. Optimal quadrature spectrum. The optimal experimental spectrum (blue) is compared with model predictions both with (solid red) and without (dashed red) a phase noise contribution. Squeezed fluctuations are observable both below and above the mechanical resonances, reflecting the two regions evident in Fig. 3. While the inclusion of phase noise in the model drastically improves the agreement with the experimental spectrum, its effect is almost negligible in the squeezed regions. As in Fig. 2, the green line indicates the spectrum of vacuum fluctuations.

of 0.9816 ± 0.0006, i.e., $\simeq$2% below vacuum fluctuations. Integrated over a similar bandwidth, the vacuum fluctuations are estimated to be 1.0001 ± 0.0027, giving a high statistical significance to the observed squeezing. This squeezing is achieved through two oscillators with occupation numbers well below unity.

Observation of squeezing requires the optical field backaction to provide a significant contribution to the total motional variance in order for the correlations between quadratures to emerge. However, increasing the backaction strength also increases the radiation-pressure noise acting on the oscillator, leading to additional heating of the motion. Furthermore, one of the main limits remains the overall detection efficiency. Tracing back to the cavity output, the ideally available squeezing would double to 4%, which means that homodyne detection in combination with a variational approach [40] can prove advantageous, at the cost of providing a less comprehensive measurement. An additional factor of 2 improvement can be obtained changing the cavity configuration from symmetric to single ended, thus reaching $\sim$8%. Finally, in the experimental results presented here collisions with background gas still represent a relevant fraction of the total heating rate. Thus the observable squeezing can potentially be further increased (up to a factor of 2) by reaching the photon recoil limit. To move past this barrier, a more sophisticated approach will be necessary. For example, adding a weak probe field would allow to implement a quantum nondemolition measurement of the field fluctuations [41].

In conclusion, we have demonstrated optical squeezing mediated by two mechanical oscillators simultaneously cooled to their quantum ground state, with occupation numbers well below unity. Our results represent a significant advance in cavity optomechanics, bridging the gap between purely mechanical quantum control and nonclassical optical fields. Even if the measured squeezing is not very pronounced, several pathways for improvement are evident. Enhanced detection efficiency through improved optical collection and single-ended cavity configurations could increase

the observed squeezing by a factor of 4 or more. Reducing mechanical heating, by improving vacuum conditions, would allow access to even lower occupation numbers and a larger degree of squeezing. The implementation of quantum nondemolition measurements and variational readout schemes could further enhance the observable squeezing while reducing noise penalties inherent in heterodyne detection.

Looking forward, our platform provides a natural test bed for exploring entanglement between multiple mechanical modes [11–13], optomechanical quantum-state transfer [42,43], and alternative approaches to quantum metrology [44]. The combination of strong coupling, quantum ground-state occupation of multiple modes, and excellent control over the mechanical and optical parameters positions levitated optomechanics as a powerful system for exploring quantum mechanics at the mesoscopic scales.

ACKNOWLEDGMENTS

We acknowledge financial support from PNRR MUR Project No. PE0000023-NQSTI and by the European Commission-EU under the Infrastructure I-PHOQS "Integrated Infrastructure Initiative in Photonic and Quantum Sciences" (IR0000016, ID D2B8D520, CUP D2B8D520).

DATA AVAILABILITY

There are no publicly available research data or software supporting this manuscript. Requests for further information or data should be sent to the authors.

APPENDIX A: THEORETICAL MODEL

The optomechanical model describing the motion of the nanosphere in the transverse tweezer plane, coupled to a cavity mode, is described in Ref. [25]. In particular, the Langevin equations for the amplitude quadrature of the intracavity field and the two mechanical modes, written in the Fourier space, are given in Eqs. (7)–(9) (see Supplemental Material of Ref. [25]), and the equation for the phase quadrature P_c can be similarly obtained from Eq. (6) (see Supplemental Material of Ref. [25]). We report them below:

$$Q_c(\omega) = i[\chi_c(\omega) - \chi_c^*(-\omega)][g_x\, x(\omega) + g_y\, y(\omega)] + \sqrt{\kappa}[\chi_c(\omega) a_{\rm in} + \chi_c^*(-\omega) a_{\rm in}^\dagger], \tag{A1}$$

$$P_c(\omega) = [\chi_c(\omega) + \chi_c^*(-\omega)][g_x\, x(\omega) + g_y\, y(\omega)] + i\sqrt{\kappa}[-\chi_c(\omega) a_{\rm in} + \chi_c^*(-\omega) a_{\rm in}^\dagger], \tag{A2}$$

$$x(\omega) = 2\chi_x(\omega)[g_x\, Q(\omega) + \sqrt{\Gamma_x}\, \xi_x], \tag{A3}$$

$$y(\omega) = 2\chi_y(\omega)[g_y\, Q(\omega) + \sqrt{\Gamma_y}\, \xi_y]. \tag{A4}$$

Here, x and y are dimensionless position operators normalized to their respective zero-point fluctuations $\sqrt{\hbar/2m\Omega_j}$ [m is the mass of the nanosphere, Ω_j with $j = (x, y)$ the oscillation frequencies in the absence of optomechanical interaction], g_j are the optomechanical coupling rates, Γ_j the heating rates, and κ is the cavity width. Fourier-transformed ($\mathcal{F}$) operators are defined as $O(\omega) \equiv \mathcal{F}[O(t)] = \int O(t) e^{i\omega t} {\rm d}t$, and $O^\dagger(\omega) = \mathcal{F}[O^\dagger(t)]$, while the complex conjugate of a complex function $f(\omega)$ is denoted as $f^*(\omega)$. In the following, we will use power spectral densities (PSDs) of the operators, defined as $S_{OO} = \int \langle O^\dagger(\omega') O(\omega)\rangle \frac{{\rm d}\omega'}{2\pi}$, cross-spectral densities defined as $S_{O_1O_2} = \int \langle O_1^\dagger(\omega') O_2(\omega)\rangle \frac{{\rm d}\omega'}{2\pi}$, and symmetrized spectra $\bar{S}_{O_1O_2} = 0.5[S_{O_1O_2}(\omega) + S_{O_1O_2}(-\omega)]$. We have also defined the mechanical and optical susceptibilities

$$\chi_j(\omega) = \frac{\Omega_j}{\Omega_j^2 - \omega^2}, \tag{A5}$$

$$\chi_c(\omega) = \frac{1}{-i(\Delta + \omega) + \kappa/2}, \tag{A6}$$

where Δ is the detuning between the tweezer radiation frequency and the cavity mode. The input noise sources have spectral densities $S_{\xi_i\xi_i} = S_{a_{\rm in}^\dagger a_{\rm in}^\dagger} = 1$.

By replacing Eqs. (A3) and (A4) into Eqs. (A1) and (A2) and using the input-output relations $Q = \sqrt{\kappa}\, Q_c - (a_{\rm in} + a_{\rm in}^\dagger)$ and $P = \sqrt{\kappa}\, P_c - i(-a_{\rm in} + a_{\rm in}^\dagger)$, we can write the output field quadratures as

$$Q(\omega) = \mathcal{A}_Q(\omega) N + \mathcal{B}_Q(\omega) a_{\rm in} + \mathcal{B}_Q^*(-\omega) a_{\rm in}^\dagger, \tag{A7}$$

$$P(\omega) = \mathcal{A}_P(\omega) N + \mathcal{B}_P(\omega) a_{\rm in} + \mathcal{B}_P^*(-\omega) a_{\rm in}^\dagger, \tag{A8}$$

where we have defined

$$\mathcal{A}_Q(\omega) = \frac{i\sqrt{\kappa}\,[\chi_c(\omega) - \chi_c^*(-\omega)]}{1 - 2i[\chi_c(\omega) - \chi_c^*(-\omega)]\left(g_x^2\, \chi_x + g_y^2\, \chi_y\right)}, \tag{A9}$$

$$\mathcal{B}_Q(\omega) = \frac{\kappa\, \chi_c(\omega)}{1 - 2i[\chi_c(\omega) - \chi_c^*(-\omega)]\left(g_x^2\, \chi_x + g_y^2\, \chi_y\right)} - 1, \tag{A10}$$

$$\mathcal{A}_P(\omega) = \frac{i\sqrt{\kappa}\,[\chi_c(\omega) + \chi_c^*(-\omega)]}{1 - 2i[\chi_c(\omega) - \chi_c^*(-\omega)]\big(g_x^2\,\chi_x + g_y^2\,\chi_y\big)}, \tag{A11}$$

$$\mathcal{B}_P(\omega) = -i\left(\frac{\kappa\,\chi_c(\omega)[1 + 4\,i\,\chi_c^*(-\omega)\big(g_x^2\,\chi_x + g_y^2\,\chi_y\big)]}{1 - 2i[\chi_c(\omega) - \chi_c^*(-\omega)](g_x^2\,\chi_x + g_y^2\,\chi_y)} - 1\right), \tag{A12}$$

$$N = 2(g_x\,\chi_x\sqrt{\Gamma_x}\,\xi_x + g_y\,\chi_y\,\sqrt{\Gamma_y}\,\xi_y). \tag{A13}$$

The symmetrized spectra of the output field quadratures read

$$\bar{S}_{QQ}(\omega) = 4\big(g_x^2|\chi_x|^2\,\Gamma_x + g_y^2|\chi_y|^2\,\Gamma_y\big)|\mathcal{A}_Q(\omega)|^2 + 0.5[|\mathcal{B}_Q(-\omega)|^2 + |\mathcal{B}_Q(\omega)|^2], \tag{A14}$$

$$\bar{S}_{PP}(\omega) = 4\big(g_x^2|\chi_x|^2\,\Gamma_x + g_y^2|\chi_y|^2\,\Gamma_y\big)|\mathcal{A}_P(\omega)|^2 + 0.5\big[|\mathcal{B}_P(-\omega)|^2 + |\mathcal{B}_P(\omega)|^2\big], \tag{A15}$$

$$0.5\big[\bar{S}_{QP}(\omega) + \bar{S}_{PQ}(\omega)\big] = 4\big(g_x^2|\chi_x|^2\,\Gamma_x + g_y^2|\chi_y|^2\,\Gamma_y\big)\mathrm{Re}[\mathcal{A}_Q^*(\omega)\mathcal{A}_P(\omega)] + 0.5\,\mathrm{Re}[\mathcal{B}_Q^*(-\omega)\mathcal{B}_P(-\omega) + \mathcal{B}_Q^*(\omega)\mathcal{B}_P(\omega)]. \tag{A16}$$

The quantum efficiency η is taken into account by modifying the spectra as follows: $\bar{S}_{QQ} \to \eta\bar{S}_{QQ} + (1-\eta)$, $\bar{S}_{PP} \to \eta\bar{S}_{PP} + (1-\eta)$, $\bar{S}_{QP} \to \eta\bar{S}_{QP}$, $\bar{S}_{PQ} \to \eta\bar{S}_{PQ}$.

In the main text we have used the simplified notation $0.5(\bar{S}_{QP} + \bar{S}_{PQ}) \to S_{QP}$, $\bar{S}_{QQ} \to S_{QQ}$, and $\bar{S}_{PP} \to S_{PP}$.

APPENDIX B: STATISTICAL ANALYSIS

Additional information regarding the shot-noise calibration procedure can be found in Refs. [28,34] and in the Supplemental Material information therein. Here, we show the statistical errors associated to the shot noise and the optimal spectrum $\tilde{S}_Q^{\mathrm{opt}}$, as presented in Fig. 4 of the main text. Both spectra are reported in Fig. 5, along with the respective error bars. At its minimum, the optimal spectrum is below the shot noise by almost 7σ. However, some structures, likely due to residual laser frequency noise and contributing by less than 1%, limit the bandwidth over which the minimum is observed.

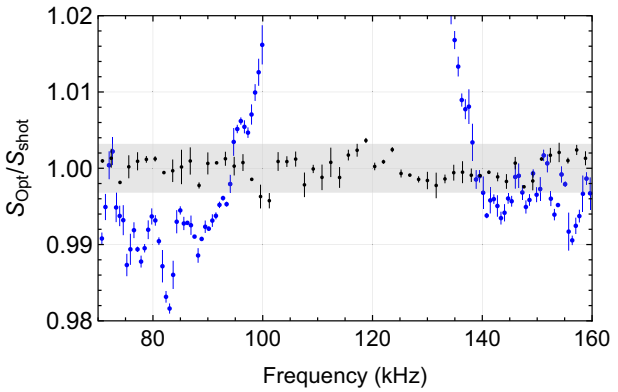


FIG. 5. Optimal quadrature spectrum (blue) compared to the measured shot noise (black). Each frequency bin of the spectra is shown with the associated error bar (1σ). The gray shaded region indicates the $\pm 2\sigma$ confidence interval of the shot-noise spectrum, demonstrating the high statistical significance of the sub-shot-noise level observed in the optimal spectrum.

[1] C. Fabre, M. Pinard, S. Bourzeix, A. Heidmann, E. Giacobino, and S. Reynaud, Quantum-noise reduction using a cavity with a movable mirror, Phys. Rev. A **49**, 1337 (1994).

[2] S. Mancini and P. Tombesi, Quantum noise reduction by radiation pressure, Phys. Rev. A **49**, 4055 (1994).

[3] J. Chan, T. P. M. Alegre, A. H. Safavi-Naeini, J. T. Hill, A. Krause, S. Gröblacher, M. Aspelmeyer, and O. Painter, Laser cooling of a nanomechanical oscillator into its quantum ground state, Nature (London) **478**, 89 (2011).

[4] T. P. Purdy, P.-L. Yu, R. W. Peterson, N. S. Kampel, and C. A. Regal, Strong optomechanical squeezing of light, Phys. Rev. X **3**, 031012 (2013).

[5] F. Marquardt, J. P. Chen, A. A. Clerk, and S. M. Girvin, Quantum theory of cavity-assisted sideband cooling of mechanical motion, Phys. Rev. Lett. **99**, 093902 (2007).

[6] M. Rossi, D. Mason, J. Chen, Y. Tsaturyan, and A. Schliesser, Measurement-based quantum control of mechanical motion, Nature (London) **563**, 53 (2018).

[7] W. H. P. Nielsen, Y. Tsaturyan, C. B. Møller, E. S. Polzik, and A. Schliesser, Multimode optomechanical system in the quantum regime, Proc. Natl. Acad. Sci. USA **114**, 62 (2017).

[8] G. Huang, A. Beccari, N. J. Engelsen, and T. J. Kippenberg, Room-temperature quantum optomechanics using an ultralow noise cavity, Nature (London) **626**, 512 (2024).

[9] J. Chen, M. Rossi, D. Mason, and A. Schliesser, Entanglement of propagating optical modes via a mechanical interface, Nat. Commun. **11**, 943 (2020).

[10] M. Bild, M. Fadel, Y. Yang, U. von Lüpke, P. Martin, A. Bruno, and Y. Chu, Schrödinger cat states of a 16-microgram mechanical oscillator, Science **380**, 274 (2023).

[11] S. Bose, K. Jacobs, and P. L. Knight, Preparation of nonclassical states in cavities with a moving mirror, Phys. Rev. A **56**, 4175 (1997).

[12] D. Vitali, S. Gigan, A. Ferreira, H. R. Böhm, P. Tombesi, A. Guerreiro, V. Vedral, A. Zeilinger, and M. Aspelmeyer,

Optomechanical entanglement between a movable mirror and a cavity field, Phys. Rev. Lett. **98**, 030405 (2007).
[13] M. Paternostro, D. Vitali, S. Gigan, M. S. Kim, C. Brukner, J. Eisert, and M. Aspelmeyer, Creating and probing multipartite macroscopic entanglement with light, Phys. Rev. Lett. **99**, 250401 (2007).
[14] F. Monteiro, G. Afek, D. Carney, G. Krnjaic, J. Wang, and D. C. Moore, Search for composite dark matter with optically levitated sensors, Phys. Rev. Lett. **125**, 181102 (2020).
[15] E. Kilian, M. Rademacher, J. M. H. Gosling, J. H. Iacoponi, F. Alder, M. Toroš, A. Pontin, C. Ghag, S. Bose, T. S. Monteiro, and P. F. Barker, Dark matter searches with levitated sensors, AVS Quantum Sci. **6**, 030503 (2024).
[16] N. Aggarwal, G. P. Winstone, M. Teo, M. Baryakhtar, S. L. Larson, V. Kalogera, and A. A. Geraci, Searching for new physics with a levitated-sensor-based gravitational-wave detector, Phys. Rev. Lett. **128**, 111101 (2022).
[17] M. Rademacher, J. Millen, and Y. L. Li, Quantum sensing with nanoparticles for gravimetry: When bigger is better, Adv. Opt. Technol. **9**, 227 (2020).
[18] U. Delić, M. Reisenbauer, K. Dare, D. Grass, V. Vuletić, N. Kiesel, and M. Aspelmeyer, Cooling of a levitated nanoparticle to the motional quantum ground state, Science **367**, 892 (2020).
[19] L. Magrini, P. Rosenzweig, C. Bach, A. Deutschmann-Olek, S. G. Hofer, S. Hong, N. Kiesel, A. Kugi, and M. Aspelmeyer, Real-time optimal quantum control of mechanical motion at room temperature, Nature (London) **595**, 373 (2021).
[20] F. Tebbenjohanns, M. L. Mattana, M. Rossi, M. Frimmer, and L. Novotny, Quantum control of a nanoparticle optically levitated in cryogenic free space, Nature (London) **595**, 378 (2021).
[21] A. Ranfagni, K. Børkje, F. Marino, and F. Marin, Two-dimensional quantum motion of a levitated nanosphere, Phys. Rev. Res. **4**, 033051 (2022).
[22] M. Kamba, R. Shimizu, and K. Aikawa, Optical cold damping of neutral nanoparticles near the ground state in an optical lattice, Opt. Express **30**, 26716 (2022).
[23] L. Dania, O. S. Kremer, J. Piotrowski, D. Candoli, J. Vijayan, O. Romero-Isart, C. Gonzalez-Ballestero, L. Novotny, and M. Frimmer, High-purity quantum optomechanics at room temperature, Nat. Phys. **21**, 1603 (2025).
[24] J. Piotrowski, D. Windey, J. Vijayan, C. Gonzalez-Ballestero, A. de los Ríos Sommer, N. Meyer, R. Quidant, O. Romero-Isart, R. Reimann, and L. Novotny, Simultaneous ground-state cooling of two mechanical modes of a levitated nanoparticle, Nat. Phys. **19**, 1009 (2023).
[25] Q. Deplano, A. Pontin, A. Ranfagni, F. Marino, and F. Marin, High purity two-dimensional levitated mechanical oscillator, Nat. Commun. **16**, 4215 (2025).
[26] A. Militaru, M. Rossi, F. Tebbenjohanns, O. Romero-Isart, M. Frimmer, and L. Novotny, Ponderomotive squeezing of light by a levitated nanoparticle in free space, Phys. Rev. Lett. **129**, 053602 (2022).
[27] L. Magrini, V. A. Camarena-Chávez, C. Bach, A. Johnson, and M. Aspelmeyer, Squeezed light from a levitated nanoparticle at room temperature, Phys. Rev. Lett. **129**, 053601 (2022).
[28] Q. Deplano, A. Pontin, F. Marino, and F. Marin, Stationary entanglement of a levitated oscillator with an optical field, Science **394**, 113 (2026).
[29] S. Mancini, D. Vitali, and P. Tombesi, Scheme for teleportation of quantum states onto a mechanical resonator, Phys. Rev. Lett. **90**, 137901 (2003).
[30] S. Pirandola, D. Vitali, P. Tombesi, and S. Lloyd, Macroscopic entanglement by entanglement swapping, Phys. Rev. Lett. **97**, 150403 (2006).
[31] M. Toroš, U. Delić, F. Hales, and T. S. Monteiro, Coherent-scattering two-dimensional cooling in levitated cavity optomechanics, Phys. Rev. Res. **3**, 023071 (2021).
[32] V. Vuletić and S. Chu, Laser cooling of atoms, ions, or molecules by coherent scattering, Phys. Rev. Lett. **84**, 3787 (2000).
[33] M. Toroš and T. S. Monteiro, Quantum sensing and cooling in three-dimensional levitated cavity optomechanics, Phys. Rev. Res. **2**, 023228 (2020).
[34] A. Ranfagni, P. Vezio, M. Calamai, A. Chowdhury, F. Marino, and F. Marin, Vectorial polaritons in the quantum motion of a levitated nanosphere, Nat. Phys. **17**, 1120 (2021).
[35] M. Aspelmeyer, T. J. Kippenberg, and F. Marquardt, Cavity optomechanics, Rev. Mod. Phys. **86**, 1391 (2014).
[36] W. P. Bowen, *Quantum Optomechanics* (CRC Press, Boca Raton, FL, 2015).
[37] K. Dare, J. J. Hansen, I. Coroli, A. Johnson, M. Aspelmeyer, and U. Delić, Ultrastrong linear optomechanical interaction, Phys. Rev. Res. **6**, L042025 (2024).
[38] A. Ranfagni, F. Marino, and F. Marin, Spectral analysis of quantum field fluctuations in a strongly coupled optomechanical system, Phys. Rev. Lett. **130**, 193601 (2023).
[39] A. Pontin, C. Biancofiore, E. Serra, A. Borrielli, F. S. Cataliotti, F. Marino, G. A. Prodi, M. Bonaldi, F. Marin, and D. Vitali, Frequency-noise cancellation in optomechanical systems for ponderomotive squeezing, Phys. Rev. A **89**, 033810 (2014).
[40] N. S. Kampel, R. W. Peterson, R. Fischer, P.-L. Yu, K. Cicak, R. W. Simmonds, K. W. Lehnert, and C. A. Regal, Improving broadband displacement detection with quantum correlations, Phys. Rev. X **7**, 021008 (2017).
[41] A. Pontin, M. Bonaldi, A. Borrielli, L. Marconi, F. Marino, G. Pandraud, G. A. Prodi, P. M. Sarro, E. Serra, and F. Marin, Quantum nondemolition measurement of optical field fluctuations by optomechanical interaction, Phys. Rev. A **97**, 033833 (2018).
[42] T. A. Palomaki, J. W. Harlow, J. D. Teufel, R. W. Simmonds, and K. W. Lehnert, Coherent state transfer between itinerant microwave fields and a mechanical oscillator, Nature (London) **495**, 210 (2013).
[43] M. J. Weaver, F. Buters, F. Luna, H. Eerkens, K. Heeck, S. de Man, and D. Bouwmeester, Coherent optomechanical state transfer between disparate mechanical resonators, Nat. Commun. **8**, 824 (2017).
[44] Q. Li, W. Li, Y. Wang, Y. Wang, L. Tian, S. Shi, and Y. Zheng, Quantum-enhanced optomechanical sensor network, Laser Photonics Rev. **20**, e01636 (2026).